Size determination and quantification of engineered cerium oxide nanoparticles by flow field-flow fractionation coupled to inductively coupled plasma mass spectrometry

L. Sánchez-García[1], E. Bolea[1], F. Laborda[1], C. Cubel[1], P. Ferrer[2], Diego Gianolio[2], I. da Silva[3], J.R. Castillo[1].

[1] Group of Analytical Spectroscopy and Sensors (GEAS). Institute of Environmental Sciences (IUCA). University of Zaragoza, Pedro Cerbuna 12, 50009 Zaragoza, Spain.

[2] Diamond Light Source, Harwell Science and Innovation Campus, Chilton, Didcot OX11 0DE, UK.

[3] ISIS Facility, Rutherford Appleton Laboratory, Chilton, Oxfordshire OX11 0QX, UK.

*Corresponding author e-mails laurasg@unizar.es, laura.biomarkers@gmail.com, Tel. + (34) 976 761 289, Fax. + (34) 976 761 292

Abstract

Facing the lack of studies on characterization and quantification of cerium oxide nanoparticles (CeO_2 NPs), whose consumption and release is greatly increasing, this work proposes a method for their sizing and quantification by Flow Field-Flow Fractionation (FFFF) coupled to Inductively Coupled Plasma-Mass Spectrometry (ICP-MS). Two modalities of FFFF (Asymmetric Flow- and Hollow Fiber-Flow Field Flow Fractionation, AF4 and HF5, respectively) are compared, and their advantages and limitations discussed. Experimental conditions (carrier composition, pH, ionic strength, crossflow and carrier flow rates) are studied in detail in terms of NP separation, recovery, and repeatability. Size characterization of CeO_2 NPs was addressed by different approaches. In the absence of feasible size standards of CeO_2 NPs, suspensions of Ag, Au, and SiO_2 NPs of known size were investigated. Ag and Au NPs failed to show a comparable behaviour to that of the CeO_2 NPs, whereas the use of SiO_2 NPs provided size estimations in agreement to those predicted by the theory. The latter approach was thus used for characterizing the size of CeO_2 NPs in a commercial suspension. Results were in adequate concordance with those achieved by transmission electron microscopy, X-ray diffraction and dynamic light scattering. The quantification of CeO_2 NPs in the commercial suspension by AF4-ICP-MS required the use of a CeO_2 NPs standards, since the use of ionic cerium resulted in low recoveries (99±9 % vs. 73±7%, respectively). A limit of detection of 0.9 μg L^{-1} CeO_2 corresponding to a number concentration of $1.8x10^{12}$ L^{-1} for NPs of 5 nm was achieved for an injection volume of 100 μL.

1. Introduction

Nanotechnology is developing rapidly in numerous industries such as chemistry, medicine, energy, computer sciences, or optics, with the consequent increase in the manufacturing of synthetic nanoparticles (NPs). Great part of the NPs interest derives from their size (1-100 nm) [1], which provides them with interesting properties such as high specific surface area, rapid diffusion or high reactivity in liquid and gas phase. It is indeed owed to their size and the resulting particular properties that questions about their potential toxicity and environmental impact also emerge [2], given the high mobility and rapid transport they exhibit in the environment and inside the body. While the consumption of engineered nanomaterials grows, the release of NPs, their evolution and interaction with the natural media and organisms is insufficiently understood. Nanomaterials may pose new risks as a result of their novel properties. In view of this potential hazard, regulatory and scientific assessment requires an understanding of exposure to both humans and the environment. Characterizing and tracking NPs in the environment is a priority for the responsible-sustainable development of nanotechnology.

Cerium oxide nanoparticles (CeO_2 NPs) have different applications in multiple fields (polishing, catalysis, UV blocker, electronics, environmental remediation, sensing, biomedicine, etc.) [3], as a consequence of their interesting mechanical, spectroscopic, catalytic and oxidant/antioxidant properties [4,5]. Most of the uses of CeO_2 NPs are related to their catalytic and sorption properties. For instance, the automotive industry uses the oxygen buffering capacity of the CeO_2 NPs to catalyse the fuel oxidation in diesel engines, where combustion tends to be incomplete. This results into lower consumption of fuel and

lower emission of soot particles and toxic gases [6,7]. Beyond the positive effects on air quality, little is known about the intrinsic toxicity of the CeO_2 NPs released to the environment. At the time nanotoxicology deals with the CeO_2 NPs hazards, efforts should be also devoted to determine the physicochemical properties responsible for their potential toxic effect.

The physicochemical characterization of CeO_2 NPs entails a series of analytical challenges related to their size, nature, and physicochemistry in aqueous phases, as well as to the expected low concentration in environmental samples. Although little information is available to date on the likely concentrations of CeO_2 NPs that end up in the environment, estimations for aquatic environments are in the range of 0.005-1.0 μg/L of CeO_2 [8], where the highest value predicted based on current usage of ceria as a fuel additive in the UK is 0.37 μg/L of CeO_2 [9]. Ecotoxicological studies use diverse analytical techniques for characterizing NPs, to understand the mechanisms and extent of toxicity of the CeO_2 NPs in relation to their properties [10,11,12,13,14]. Among all, particle size has been pointed as a key property for determining the toxicity of CeO_2 NPs [e.g. 12,13] in relation to differences in the surface area. The complexity of the CeO_2-NPs suspensions and the limitations of the analytical techniques lead to diverse operative problems. For instance, Microscopy-based techniques such as Transmission Electronic Microscopy (TEM) or Atomic Force Microscopy (AFM) show limitations for measuring individual sizes in samples of inherent instability and sample-preparation protocols promoting agglomeration [15]. Similarly, Dynamic Light Scattering (DLS), ideally developed for monodisperse populations, present inconveniences for measuring unknown, polydisperse samples. This

technique, requiring concentrations of NPs in the range of mg L^{-1}, may not be very useful for characterizing NPs in natural environments or biological media, where typically neutral pH values promote the CeO_2 NPs agglomeration [15]. Brunauer–Emmett–Teller (BET) surface-area measurements assuming spherical shape of the NPs may underestimate the surface area, thus leading to the overestimation of particle size [16]. Size measures from X-Ray Diffraction (XRD) have limited value in the case of polydisperse samples with amorphous components. While size determinations by XRD and BET are not directly relevant in aqueous media (i.e. done on solid samples), they provide relevant information for understanding the effect of the medium on NP properties [15]. All in all, the instability of CeO_2 NPs in common environmental medium (i.e. aqueous suspension) and the multiple analytical limitations described above reveals the necessity for developing novel analytical tools and sample preparation protocols to standardize the characterization of CeO_2 NPs, where robust and sensitive methods providing low limits of detection are required.

The present study proposes the use of Flow Field-Flow Fractionation (FFFF) coupled to Inductively Coupled Plasma – Mass Spectrometry (ICP-MS) for the size characterization and quantification of CeO_2 NPs. Despite FFFF is a family of powerful techniques for size characterization of NPs of diverse nature [17], there is a lack of studies dealing with the quantification of CeO_2 NPs, largely due to the lack of certified size standards of CeO_2 NPs and the poor stability of these NPs in suspension. We have investigated different conditions and separation factors affecting the stability of the CeO_2 NPs in suspension, and discussed different size-calibration strategies. We pose the FFFF-ICP-MS tandem as an alternative to other commonly used techniques, where results are limited by sample amount requirements or hydrodynamic stability. The performance of two FFFF separation modes (Asymmetric

Flow Field-Flow Fractionation and Hollow Fiber-Flow Field-Flow Fractionation) is evaluated here in the search of the best response in terms of resolution and recovery. This study constitutes the first application of size characterization of CeO_2 NPs by FFFF techniques and aims at exploring the capabilities of this analytical tool for quantifying CeO_2 NPs at environmental relevant concentrations, given the good sensitivity of ICP-MS for metal-containing NPs.

2. Experimental

2.1. Chemicals

Two different carriers were studied, one containing an ionic surfactant (sodium dodecyl sulfate, SDS) and the other consisting of a commercial mixture of nonionic and ionic detergents (mixed surfactant). The carriers were prepared by dissolving the corresponding mass of SDS (Merk, Darmstadt, Germany) and mixed surfactant (Novachem Surfactant 100, Postnova Analytics) in ultrapure water obtained from a Milli_Q Advantage system (Millipore, Bedford, MA, USA). Diluted solutions of sodium hydroxide (Merck, analytical grade) and nitric acid (J.T. Baker, trace metal analysis, 69-70%) were used to adjust the carrier pH. Nylon 0.2 μm filters (Millipore, USA) were used for filtering the carrier.

2.2. CeO_2 nanoparticles

Two commercial suspensions of cerium oxide NPs were used for method optimization. STD-4 (5 wt. % aqueous suspension 0.01 M HNO_3) had a nominal average size of 4 nm and was purchased from PlasmaChem (Berlin, Germany). STD-10 (20 wt. % aqueous

suspension, 2.5 % acetic acid), with nominal average size of 10-20 nm, was obtained from Sigma-Aldrich (Saint Louis, USA).

A commercial suspension (NanoArc®, CAS: 1306-38-3) supplied by Alfa Aesar (Karlsruhe, Germany) for polishing purposes (e.g. in ultrafine acid side polishing slurries) was used as sample for testing the size characterization and quantification methods. The product is provided by the manufacturer as colloidal suspension of ceria NPs (25 wt. % in H_2O, pH 3.5), with a nominal BET size of 30 nm for the dry powder.

Diluted suspensions of CeO_2 NPs (10 or 50 mg L^{-1}) were prepared by further dilution of the commercial products with the corresponding carrier. These dilutions were prepared from suspensions of intermediate concentration of CeO_2 NPs (ca. 2,000 mg L^{-1}), in similar conditions as provided by the manufacturers (i.e. HNO_3 0.01M). The CeO_2 NPs were stable in the acidic conditions for at least one month. Dilutions with carriers were freshly prepared prior to each measurement and subsequently analyzed within the next hour since preparation, where the risk for aggregation was observed to be minimum. Stability of bulk and intermediate suspensions, as well as suspensions diluted with carriers, was periodically checked by UV-vis absorption spectrophotometry.

2.3. Flow field-flow fractionation-inductively coupled plasma mass spectrometry (FFFF-ICP-MS)

The FFFF system used was an AF2000 (Postnova Analytics, Landsberg, Germany), run in two modes: a) Asymmetric Flow Field-Flow Fractionation (AF4), and b) Hollow Fiber-Flow Field-Flow Fractionation (HF5). In AF4 mode, separation is achieved by applying a transverse, unidirectional cross-flow towards a flat membrane. This system used a

trapezoidal channel of 27.5 cm in length and from 2 to 0.5 cm in width, with spacers of 190 μm or 350 μm. The channel thicknesses were determined experimentally for each spacer used by injecting NaN_3 (Sigma-Aldrich, Saint Louis, USA; 100 μl, 0.1 % (w/v) in carrier) [18]. The eluting peak was detected by the UV-Vis detector (at 254 nm) at a fixed channel flow rate of 0.5 mL min^{-1} and a minimum crossflow of 0.01 mL min^{-1}. Experimental values of 189±9 μm and 319±4 μm were obtained for the spacers of 190 μm and 350 μm, respectively. Ultrafiltration membranes of polyether sulfone (PES) with a cutoff of 5 kDa (Postnova Analytics) were used as the accumulation wall (Table 1). The effect of the carrier composition (SDS vs. Novachem) on the size separation and NPs-membrane interaction was tested at different concentrations (0.01, 0.05 and 0.1% v/v). The surfactant solutions prepared in ultrapure water adjusted to pH 10 were used as FFFF carrier, which was degassed prior to use by an online vacuum degasser. Different crossflow programs were studied. Table 1 summarizes the optimal program found for AF4. Manual injections were performed using sample loops of 20 and 100 μL. The sample mass injected was controlled to minimize overloading effects. Multiple runs with different concentrations (from 1 to 100 mg L^{-1}) of CeO_2 NPs (STD-4 and STD-10) were performed. No significant effects on retention time were observed for concentrations below 50 mg L^{-1}, which correspond to a total mass injected of 5 μg.

In HF5 mode, the same sample volume is injected and separation is attained by applying a radial cross-flow towards a porous fiber wall (hollow fiber cartridge made of a 10 KDa PES membrane) in a cylindrical channel of 800 μm diameter (Postnova HF-28AN Hollow Fiber C). The low channel volume (typically < 100 μL) in HF5 entails a lower dead volume and solvent consumption than in AF4. Following recommendations from Postnova Analytics,

the previously established method on AF4 was transferred to HF5 for further development and optimization (Table 2).

In both modes, the eluent was directed from the channel/hollow fiber through a UV–Vis diode-array detector (Shimadzu, Duisburg, Germany) recording the signal between 200 and 650 nm, where the maximum absorption for CeO_2 NPs was observed to be around 290 nm. A complete spectrum of the eluent was registered every 2 s. For the elemental detection, the FFFF system was coupled to an ICP mass spectrometer (ELAN DRC-e, PerkinElmer, Toronto, Canada). The outflow from the system was delivered directly to the nebulizer of the spectrometer—a glass concentric slurry nebulizer with a cyclonic spray chamber (Glass Expansion, Melbourne, Australia) was used. The ICP-MS data acquisition was performed on ^{140}Ce isotope, using 20 sweeps per reading and a dwell time of 50 ms. Default values were used for the rest of instrumental parameters.

2.4. FFFF size calibration procedure

Particle size calibration was performed by using two different methods. The first one was based on the FFFF theory (see Section S1 in Supplementary Information), where using appropriate equations allow to relate the retention parameters with the diffusion coefficient (and thereby the hydrodynamic size) [e.g. 18,19,20,21,22]. This approach required the measurement of the experimental channel width, which was obtained by measuring the elution time of an unretained substance (i.e. sodium azide) or through the retention time of a substance of known diffusion coefficient (i.e. Au NPs). A single monodisperse suspension of Au NP (NIST, Gaithersburg, USA) of 60 nm was employed for the latter means. The second method was based on the use of size standards, so that the relationship

between retention time and size can be established for fixed flow conditions [e.g. 23,24,25,26]. Single monodisperse suspensions of Ag NPs (10 nm from PlasmaChem, Berlin, Germany; 40 nm and 100 nm from Sigma Aldrich, Saint Louis, USA), and SiO_2 NPs (10 nm and 20 nm from PlasmaChem, Berlin, Germany; and 150 nm from Sigma Aldrich, Saint Louis, USA) were injected and their known size (core-particle size) plotted against the resulting retention ratio R. The curve-fitting equations were then determined for the two NP types according to Eq. 1:

$$log\ R = a \cdot log\ d + b \quad (1)$$

Where R is the retention ratio (ratio of the elution time of the void peak, t_0, and the analyte, t_r), a is the y-intercept, b the line slope, and d is the NP core diameter.

2.5. Cerium determination in commercial suspensions

All determinations of total cerium were conducted by Inductively Coupled Plasma – Atomic Emission Spectroscopy (ICP-AES), after microwave-assisted acid digestion (Mars 5, CEM Corp.). First, a volume of 4 mL of HNO_3 (65%) was added to ca. 0.5 g of sample in the digestion vessels, temperature ramped in 15 min to 210ºC by applying a power of 800W, and then maintained at 210ºC for another 15 min. In a second step, a volume of 1.5 mL of H_2O_2 (30%) was added to the mixture, allowing for reaction during 15 min, then the same microwave program was applied. The digested samples were diluted to 20 mL with milli-Q water and total cerium concentrations in the diluted samples determined using ICP–AES (Iris Intrepid Radial Thermo Corporation).

2.6. Transmission Electron Microscopy (TEM)

Samples were prepared on carbon-coated 300 mesh copper grids for TEM analysis. A volume of ca. 10 μL of the cerium oxide suspensions were dropped on the grid and left to dry completely. Images were obtained by using a TEM instrument (Tecnai G2-F30 Field Emission Gun microscope) that worked at 300kV with a super-twin lens and 0.2 nm point-to-point resolution and 0.1 line resolution. The microscope was equipped with an energy-dispersive X-ray analysis system (INCA 200 X-Sight, Oxford Instruments) for elemental analysis and element localization on the samples. The size of individual NPs was studied on images recorded with a GATAN CCD camera and subsequently analyzed with ImageJ 1.47 v. (National Institute of Health, USA). About 500 particles were examined per sample, by analyzing at least 100 particles/image in five images. These data were treated with Excel to obtain size histograms, where the number frequency of size intervals were plotted.

2.7. DLS and zeta potential measurements

DLS measurement conditions are detailed in Section S2 of the Supplementary Information. Measurements of the zeta potential were conducted with a Brookhaven 90Plus DLS instrument (Brookhaven Instruments, Holtsville, NY, USA). A volume of the ceria-NP size standards was pumped into the cuvette of the photon correlation spectrometer provided with a dip-in (Uzgiris-type) electrode, and measured the zeta potential once the pH (2-12) had been adjusted in an automated titration cell. The zeta potential results are expressed as mean of five measurements taken at each pH value.

2.8. FFFF recovery calculations

Recovery calculations were done using three injections of standard or sample in absence of channel in the FFFF system. Then, injections applying some of the injection or crossflow

programs were conducted. Afterwards, peaks areas were calculated from the signal, with the recoveries being expressed as:

$$R\,(\%) = S/S_0 \cdot 100 \qquad (2)$$

where S is the signal area obtained when a crossflow is applied and S_0 is the signal area obtained with no crossflow. Recoveries were calculated from the absorbance signal at the maximum wavelength (i.e. 290 nm) and ^{140}Ce ICP-MS signals.

2.9. AF4-ICP-MS Quantification procedure

Quantification of CeO_2 NPs separated by AF4-ICP-MS was performed by external calibration using standard suspensions of CeO_2 NPs prepared from STD-10 and the corresponding peak areas. Calibration standards were injected in flow injection mode, in absence of channel at different mass concentrations. The sample (i.e. commercial suspension from Alfa Aesar) was injected under the optimal separation conditions described in Table 1. Quantification was based on the integration of the fractogram and subsequent interpolation in the corresponding calibration curve, following the procedure described in [27].

3. Results and discussion

3.1. Study of the conditions for stabilization of CeO_2 nanoparticles

The size characterization of any NP suspension requires of the NPs stability under the experimental conditions used. Although the suspensions of CeO_2 NPs provided by the manufacturers are supplied as stable suspensions, any change in the environment

surrounding of the NPs may lead to aggregation. The stability of the NPs in suspension may be conditioned by variables such as pH, ionic strength, or presence of surfactants. In FFFF, the injection and focusing processes during measurements may also lead to aggregation processes. Therefore, the selection of the working conditions, including carrier composition and FFFF operational parameters (e.g. time of injection/focusing or crossflow rate), should be done carefully in order to minimize the risk of aggregation.

One of the key factors determining the NPs stability in aqueous suspension is the pH, since it determines the zeta potential of the NPs in the medium. Here, the study of the electrophoretic mobility of CeO_2 NPs at concentrations of 50 mg L^{-1} allowed determining isoelectric points at pH of 6.7 and 7.0 for the standard suspensions STD-4 and STD-10, respectively (Fig. 1), in agreement with values reported elsewhere [e.g. 28,29,30]. Stability requires of the highest repulsion between the NPs themselves and with the membrane to avoid aggregation or adsorption phenomena. In this case, higher repulsion is favored at extreme pH values, where the zeta potential is higher (absolute value $\geq$20 mV). In principle, the easiest conditions to operate would be acidic, such as those of the commercial standard suspensions (i.e. pH 2-3). However, at those pHs the CeO_2 NPs are positively charged (Fig. 1), while the PES membrane presents negative charge [31], thus causing mutual attraction. This effect was manifested in form of small, wide and tailed peaks that indicated attractive interactions between the NPs and PES membrane (data not shown). As the PES zeta potential becomes more negative as pH increases [31], basic pHs seems more suitable for providing the needed repulsion with the ceria NPs. Therefore, a pH value of 10 was chosen to operate here, as it ensures the electrophoretic stability of the CeO_2 NPs in

suspension. The use of higher values of pH is limited as the ceramics frits underlying the channel tend to be corroded [18].

The addition of surfactants to the carrier is a common practice in AF4 in order to increase the suspension stability. The presence of ionic and nonionic surfactants contributes to create electrostatic or steric repulsion, by changing the surface charge of the dispersed phase or by forming an adsorbed layer onto the NPs that balances attractive and repulsive forces, respectively. Here, SDS was chosen as an ionic surfactant, whereas the mixed surfactant Novachem was selected as a combination of ionic and nonionic surfactants. Different volume concentrations of surfactant (0.1%, 0.05%, 0.01%) were tested. The use of high concentration of surfactant (0.1%) caused the suspensions to become foamy and cloudy for the two carriers tested, which suggested the formation of aggregates. The elution of a small, narrow peak of CeO_2 NPs in AF4 overlapping the void peak (data not shown), suggested the formation of large aggregates of CeO_2 NPs eluting on steric mode. This effect was not observed at lower concentrations of SDS or Novachem (0.05% or 0.01%; Fig. 2) as discussed below.

3.2. Effects of separation conditions on recovery and peak shape.

The proper characterization and quantification of CeO_2 NPs requires of adequate separation conditions, together with high recoveries and repeatability of the measurements. Minimizing possible interactions between the NPs and the channel components is crucial for a good recovery of the samples, since irreversible processes may lead to NPs losses in the FFFF system. The carrier composition is one of the parameters affecting these interactions. Also the presence of ionic and/or nonionic surfactants in the carrier may be

decisive for obtaining a good separation of peaks. Here, the effect of using different concentrations of ionic and mixed surfactants was tested for separation and recovery purposes.

Figure 2 shows the fractograms obtained for STD-4 in three different carrier compositions under the same separation conditions. The use of diluted anionic surfactant (0.01% SDS) produced a wide peak, with two maxima at 7 and 14.5 min (Fig. 2a) and a recovery value of 23% (Table 3), calculated according to Eq 2. A higher SDS concentration (0.05%) produced a narrower peak completely eluted before 15 min with a single maximum at 6 min (Fig. 2b) and recoveries close to 70% (Table 3). The same concentration for the mixed surfactant Novachem gave a peak with a maximum at the same time (6 min), but with a second distribution at 11 min (Fig 2c), similarly to the fractograms obtained with SDS 0.01% although with higher recovery in this case (100%; Table 3). These results were compared with the size distribution observed by TEM. The size histogram showed a homogeneous size distribution with most of the NPs in STD-4 having a diameter between 2 and 3 nm (Fig. 3a), with the lowest size attainable at the highest magnification being 1.2 nm. Therefore, the presence of two different populations observed with SDS at 0.01% and Novachem at 0.05% was interpreted in the light of instability of the suspensions in those media, likely leading to the formation of aggregates eluted at longer times.

The recovery of the CeO_2 NPs with 0.05% SDS was compared for the two studied standards (Table 3). Higher values were always obtained for STD-10, what suggested lower interactions between these NPs and the channel membrane relative to the NPs in STD-4. This difference was not explained by the electrostatic repulsions predicted from the z-potential values that were similar for the two standards at pH 10 (Fig. 1). However, distinct

surface composition of the two NPs would justify the different recoveries observed, while the loss of the smallest NPs in STD-4 through the membrane cannot be discarded [e.g. 18].

The repeatability of measurements was observed to be adequate for 0.05% SDS, with variations of the retention time of 1% for both STD-4 and STD-10. It is noteworthy that the recoveries in Table 3 correspond to the analyses performed after a first conditioning injection. According to [32], conditioning the membrane with a first injection of sample may be important for reducing undesirable adsorption phenomena. Here, the conditioning effect was observed when the lowest recovery obtained during the first injection improved considerably in the subsequent measurements, as observed elsewhere for Ag NP [27].

The increment of the ionic strength by the addition of $NaNO_3$ up to 5 mM did not affect the fractogram profile (data not shown), whereas the recoveries obtained were slightly lower (Table S1). This suggests that the shielding effect caused by the increment on the ionic strength did not affect the separation of the CeO_2 NPs, and repulsions with the permeation membrane were strong enough to avoid a larger adsorption of the NPs.

Considering the fractogram profiles, the recoveries, and repeatability obtained for the two CeO_2 standards, 0.05% SDS was chosen to be the most adequate carrier composition for further studies.

3.3. *Effect of separation conditions on resolution*

One of the main advantages of AF4 is its versatility for adapting the separation conditions in function of the nature of the species to be characterized. At the same time, this versatility implies the study of the working conditions for every kind of sample, with the difficulty to find a good compromise of working conditions for different situations [17]. In this work,

we tested the effect of the spacer thickness (w) on the elution time of the two CeO_2 standards (Fig. 4a-b). On one hand, the FFFF theory predicts a direct dependency of the elution time on w^2 (see Section S3 of Supplementary Information), so that longer retention times are expected for thicker spacers. On the other hand, it is also accepted that thinner channels improve the relative fractionating power in AF4 [33]. In this study, the use of a 190 μm spacer resulted into very similar elution times for the CeO_2 NPs in STD-4 (5.6 min) and STD-10 (5.8 min) (Fig. 4a), likely due to the similarity of both size distributions as deduced from the analysis of their TEM images (see Fig. 3) and the short elution times under the separation conditions selected. With a 350 μm spacer, a slightly better separation was obtained for STD-4 (7.9 min) and STD-10 (10.5 min), although at the expense of the peak width (4-9-fold wider than with the 190 μm spacer; Fig. 4b). The samples recoveries were comparable with both spacers (Table 3). On the basis of these results, the 350 μm spacer seems more adequate for obtaining better resolution, while the 190 μm spacer provides shorter fractograms, what may be suitable for working with large CeO_2 NPs as long as counting on well-differentiated size standards.

Elution times [19] and resolution [34] can be also modulated by optimization of the crossflow rate (V_c) and flow rate out of the channel (V_{out}), although recoveries can be compromised at high V_c, and V_{out} is experimentally limited by the pressure inside the channel (1.3 mL min^{-1} with the present system). Here, different values of V_c (0.325-1.000 mL min^{-1}) and V_{out} (1.0-1.3 mL min^{-1}) were tested for STD-4 (Fig. S1). The highest and narrowest peak was obtained for V_c=0.325 mL min^{-1} and V_{out}=1.0 mL min^{-1} (Fig. S1a), while different combinations of increasing V_c and V_{out} (i.e. maintaining or increasing the

V_c/V_{out} ratio) produced a progressive broadening and deterioration of the peaks shape (Fig. S1 b-d), although with similar recoveries. Thus, a V_c/V_{out} ratio of 0.325 allowed correct separation of the NPs from the void peak, obtaining total elution times shorter than 30 min with recoveries >70%.

3.4. Hollow Fiber versus Asymmetric Flow Field-Flow Fractionation.

Compared to standard AF4 channels, hollow fibers (HF5) work with reduced membrane areas causing high separation forces at lower crossflows, thus involving lower consumption of carrier and production of wastes. Here, the AF4 method (Table 1) was transferred to the HF5 system for method development. According to the manufacturer, transferring separation conditions from the standard AF4 to HF5 generally needs of applying conversions factors empirically determined at 0.5 for V_c and 0.75 for V_{out}, likely requiring of further method development. We started testing the rate values resulting from applying the recommended conversion factors (i.e. V_c=0.1 mL min^{-1} and V_{out}=0.75 mL min^{-1}) on STD-4, but no peak was detected under these conditions. Decreasing V_c to 0.05 mL min^{-1} and increasing V_{out} to 1.0 mL min^{-1} allowed to improve the peak shape with a recovery of 90% (Table 3). Alternatively, the simultaneous increase of V_c to 0.05 mL min^{-1} and V_{out} to 1.3 mL min^{-1} (V_c/V_{out} ratio of 0.038) resulted into narrower peaks eluted at shorter times, although with lower recovery (64%). The further decrease of V_c to 0.02 mL min^{-1} at different combinations of V_{out} (1.0, 1.2, and 1.3 mL min^{-1}) produced wider and more dispersed peaks (recoveries of about 70%). Therefore, the parameters providing the best results with HF5 in terms of peak shape and recovery were V_c=0.05 mL min^{-1} and V_{out}=1.0 mL min^{-1} (Table 2).

In terms of resolution, CeO_2 NPs standards in HF5 were eluted intermediately compared to AF4, depending on the spacer used (Fig. 4). STD-4 was eluted always later with HF5 (t_r=8.0 min) than with AF4 (t_r=5.6 min and 7.9 min, with 190 μm and 350 μm, respectively). In contrast, STD-10 was eluted with HF5 (t_r=8.9 min) in between the times obtained with the 190 μm (t_r=5.8 min) and 350 μm (t_r=10.5 min) spacers. In terms of peak shape, HF5 produced peaks of similar width to those derived from using AF4 with a 350 μm spacer (Fig. 4). On the basis of these results, we propose the use of one or another method depending on the particular samples and resolution needs, being aware of the performance and limitations of each modality. While AF4 with a 190 μm spacer offers good performance in terms of peak shape and short fractograms, the use of a 350 μm spacer provides higher resolution though decreasing the fractograms quality, under the same flow conditions. In between, HF5 offers intermediate resolution and peak shapes.

3.5. *Size determination of CeO_2 nanoparticles in a commercial nanoceria suspension.*

Two different approaches were used for size characterization of the commercial nanoceria suspension by FFFF; one based on the FFFF theory, by the estimation of channel thickness (*w*) (see section S1 of Supplementary Information), and another based on the use of size standards (see section 2.4 of Experimental). In order to compare the results obtained, the range of sizes of the CeO_2 NPs in STD-4, STD-10, and the commercial suspension were previously determined by different ancillary techniques (Table 4). According to TEM analysis, STD-4 and STD-10 are relatively monodisperse suspensions, showing size ranges from 1 to 5 nm and from 1 to 10 nm core particle diameters, respectively. Mode values of the number-based histograms obtained by the analysis of TEM images (Fig. 3) are in good

agreement with the average values obtained by XRD analysis in both cases (see Section S4 and Table S2 in the Supplementary Information). Hydrodynamic diameters measured by DLS were also in concordance with the TEM and XRD values (Table 4), probably due to the absence of capping agents or molecules sorbed to their surface in HNO_3 (0.01% v/v) [35]. In any case, the DLS sizes were in the upper limit of those determined by XRD or TEM, as expected from being hydrodynamic diameters versus the physical sizes measured by TEM or XRD. The commercial suspension showed a larger polydispersity, according to TEM images (Fig. 5), with particle sizes within a range from 2 to 65 nm of different shapes, similar to those values reported elsewhere [36] by means of Raman and electrochemical analysis. The analysis of TEM images was not possible with the software used (described in the experimental section) due to the large heterogeneity in shape and size of the NPs in the commercial suspension, so no histogram was obtained for this sample. Comparing the sizes obtained with XRD (40 nm average crystalline diameter) and DLS (26 nm hydrodynamic diameter) (Table 4), it can be stated that DLS failed to give a representative average value for this commercial suspension. The different shapes found in this product, together with its larger polydispersity, would justify the differences observed.

The results obtained by FFFF following different strategies for STD-10 and the commercial suspension are shown in Table 5. The first row represents the hydrodynamic diameter obtained according to the FFFF theory and based on Eq. 6 (Section S1 of the Supplementary Information). The value predicted for STD-10 as mean ± standard deviation of the particle size distribution derived from fractograms (16±8 nm, Table 5; mass-size distribution shown in fig. S3) is within the range given by the manufacturer (i.e. 10-20 nm). The differences observed with respect to the TEM and XRD values (i.e. 4 nm and 5 nm,

respectively; Table 4) reflect changes in hydrodynamic diameters in the carrier media respect to core diameters. In this regard, the CeO_2-NPs suspensions were analyzed by DLS in the AF4 carrier medium. An increment on hydrodynamic diameters was observed in both STD-10 and the commercial suspension (data not shown) relative to the original suspensions (i.e. HNO_3 0.01M), although some inconsistencies were obtained in the average values, probably due to the lower concentrations needed for ensuring the stability of the suspensions in the AF4 carrier. Besides, number size-based distributions measured by DLS in samples of high polydispersity can be biased toward larger particle size due to the size dependent scattering intensity and the way the correlation function is obtained [37].

The NIST Au-NP reference material (60 nm) was also used to estimate experimentally the channel thickness (*w*) as described in [22]. Results obtained according to this procedure are summarized in the second row of Table 5. The *w* estimate obtained (189 μm) is far from both the expected value and the value obtained with azide. This suggests that Au NPs are not eluted under the conditions predicted by the FFF theory or that a significant modification of the hydrodynamic dimensions in the carrier is produced. Consequently, larger values for both STD-10 (29±14 nm) and the commercial suspension (81±35 nm) were obtained respect to those predicted by the first procedure.

For the size calibration with NP standards, different NPs suspensions of known size can be used. A commonly used size reference standard are the traceable polystyrene-latex (PCL) beads or spheres [21,24,26,38,39]. Ideally, calibration with size standards of different composition requires elution times solely determined by their diffusional behaviour, so FFFF run conditions have to be optimized separately for both size standards and samples [40]. Alternatively, the use of NP suspensions of the same composition as that of the

sample NPs has been also reported [27,41]. In this case, the potential interactions between sample NPs and accumulation wall that can affect the elution behaviour (such as van der Waals forces [42] or electrostatic interactions [43]) are theoretically compensated, since both standards and sample NPs behave similarly. In fact, Gigault and Hackley [42] have demonstrated a clear influence of the core NP material nature on the retention process in the AF4 channel. Here, Ag NPs, which size had been well characterized by FFFF in previous studies [e.g. 27,44], were used as metal size standards, while SiO_2 NPs were employed due to their similarity to CeO_2 NPs in terms of chemical nature and z-potential [e.g. 26,27] at the selected pH values. Results are shown in the next rows of Table 5. According to the calibration against Ag standards, the size distribution of CeO_2 NPs in STD-10 showed diameter values of 36±20 nm at peak maximum. This estimation was similar to that obtained when calibrating with the NIST Au NPs (29±14 nm), and about two times the value predicted by the theory (i.e. 16±8 nm). These discrepancies respect to the theoretical predictions confirm a different behaviour of Ag NPs in the separation channel relative to the CeO_2 NPs, despite their similar size [42], leading us to discard their use for size calibration.

Aiming at the greatest similarity to the analyte, the feasibility on the use of oxide nanoparticles (i.e. SiO_2 NPs) as size standards was studied [26,45]. Injecting the SiO_2 standards in AF4 under the same separation conditions as the analyte (Table 1), resulted into size estimations of the STD-10 NPs of 16±11 nm, as that predicted by the theory (Table 5). The calibration versus SiO_2 NPs of known size gave also coherent values in the case of a AF4 channel with different dimensions (i.e. spacer of 190 μm) and with a hollow fiber (21±14 nm and 20±16 nm respectively; Table 5), which confirmed the robustness of

this approach for the size estimation of CeO_2 NPs, in the absence of well-differentiated size standards of CeO_2 NPs.

The size of CeO_2 NPs in the commercial suspension was then studied following these approaches. Applying the FFFF theory, a mean hydrodynamic diameter of 47±20 nm was obtained at peak maximum (Table 5), (mass size distribution shown in Fig. 6). The use of SiO_2 NPs as size standards gave similar results, with the CeO_2 NPs size estimated to average 65±40 nm (350 μm spacer in AF4), 52±32 nm (190 μm spacer in AF4), and 57±37 nm (HF5), depending on the FFFF system used (Table 5). These results were in the same range (considering the standard deviations derived from the size distributions shown in table 5) than those observed by TEM (2-65 nm) or XRD (40 nm) (Table 4). The analysis of the EXAFS region by XAS (see Section S5 in Supplementary Information), indicated a higher atom packing level in this product compared to STD-4 or STD-10 that confirmed the largest size of the CeO_2 NPs in the problem sample (Fig. S4). The general agreement of the three FFFF results and their relatively concordance with different techniques (TEM, XRD, and DLS), considering the different nature of the size distribution measured by all these techniques, confirmed the validity of using both SiO_2 NPs of known size as size standards and the FFFF theory for estimating the size of CeO_2 NPs, and reveal the importance of applying multi-method approaches for reducing biases and ambiguous characterisation.

3.6. *Quantification of CeO_2 nanoparticles in a commercial suspension*

The direct quantification of CeO_2 NPs by ICP-MS based on the injection of ionic cerium standards was first evaluated. The total concentration of cerium in STD-4, STD-10 and the commercial suspension was firstly determined by direct analysis after microwave-assisted

acid digestion, calibrating against standards of Ce (IV) in 1% nitric acid. The results, expressed as cerium concentration recovery and compared to the direct analysis of the diluted suspensions of NPs, were determined at 58% (STD-4), 62% (STD-10), and 73% (commercial suspension) (Table 6). Independently of the NP size ranges, the concentration of cerium in the suspensions was determined by direct measurement to be between 27 and 42 % lower than that measured after digestion (i.e. 100%). This effect has been previously observed for CeO_2 and other metal NP species and the lower sensitivity for the CeO_2 NP explained by losses during the transport of the NPs into the plasma or an incomplete vaporization of the NPs [46]. Accounting for that difference is essential when online quantifying CeO_2 NPs by AF4-ICP-MS. As stated by [47], total decomposition of nanoparticles in the plasma cannot be guaranteed and hence the possibility of using the corresponding ionic standard. These authors reported the use of HNO_3 and NaOH media to improve the NPs recovery for the ICP-MS direct quantification, with quantitative recovery for CeO_2 NPs using NaOH 10^{-3} M. Here, different media (HNO_3 1% (v/v), NaOH 10^{-3} M and SDS 0.01% at pH 10) were tested for the ICP-MS analysis of both the STD-10 and the commercial suspension, to check whether recoveries could be improved during the ICP-MS quantification, although no significant differences were observed. The use of CeO_2 NP (STD-10) was then proposed as an alternative standard to the ionic cerium, given the similar nature of both NP suspensions. A calibration curve was obtained from injecting different concentrations of the quantification standard as described in section 2.9. In this case, a good recovery (97±7 %) was obtained respect to the value measured after microwave assisted acidic digestion (Table 6, second column), which confirms the goodness of the approach.

The quantification of the CeO_2 NPs by AF4-ICP-MS was based on the integration of the sample fractogram. The quantification results (expressed as recoveries) were slightly lower than the amount injected in the AF4-ICP-MS (81±3%, Table 6). This discrepancy is justified by effect of the recovery attained in the AF4 channel (82±9%), calculated according to Eq. 2 and being similar to those obtained for STD-4 and STD-10 (Table 3). Considering the low fraction of Ce below 3 kDa (<1%) measured in the commercial suspension by ultrafiltration, the losses observed likely correspond to CeO_2 NPs sorbed onto the permeation membrane [46]. All in all, using a CeO_2 suspension as standard seemed an adequate procedure for estimating the amount of size-characterized CeO_2 NPs in a problem sample, although the different behaviour of nanoceria in different suspensions when introduced directly into the plasma must be considered for accounting for differences between the quantification standard and sample. In the present study, a recovery of 99±9% in the AF4-ICP-MS quantification (once the channel recovery was corrected, as shown in last column in table 6), was achieved.

The limit of detection of the FFFF-ICP-MS system was calculated as 3 times the standard deviation of baseline divided by the sensitivity. A volume of 100 µL of a diluted suspension of STD-10 (500 µg L^{-1} Ce concentration) was injected and the peak height at the maximum of the ICP-MS fractogram was used for calculations. A value of 0.015 µg L^{-1} CeO_2 was found, which corresponds to a number concentration of $3.3x10^{10}$ L^{-1} as calculated from assuming a spherical shape of the CeO_2 NPs and a typical radium of 2.5 nm (fig. 3c), and accounting for the CeO_2-NPs density (7.13 µg·cm^{-3}; [15]) and the Ce/CeO_2 mass fraction. Besides, the potential preconcentration capabilities of FFFF by the injection of large volumes [48] could improve the determined LOD value. Therefore, the high sensitivity

achieved provides the FFFF-ICP-MS tandem with great potential for studying CeO_2 NPs in environmental samples of typically low concentrations.

4. Conclusions

This work proposes the coupling of FFFF to an ICP-MS detector for the size characterization and quantification of CeO_2 NPs. We face the lack of methods for size characterization of CeO_2 NPs, in part owed to the scarcity of certified CeO_2 NP standards and the instability of CeO_2 NPs suspensions, by proposing the application of two modalities of FFFF (Asymmetric Flow- and Hollow Fiber-Field Flow Fractionation, AF4 and HF5). In this case, AF4 has shown to be a more versatile system respect to HF5, although the later offers a ready-to-use system with a lesser carrier consumption, thanks to the lower crossflow used. Both systems showed similar channel/fibber recoveries, slightly higher in the case of HF5, likely due to the lower surface of the permeation membrane of the fibber. It can be concluded that choosing one or another should be based on the particular samples and needs of the study (i.e. differences on NP sizes, time requirements, costs).

The procedure proposed for determination of mass-based size distribution of CeO_2 NPs suspensions is based on the use of SiO_2 NPs suspensions of known diameter as size standards. Although the comparison with size values obtained by other techniques is not straightforward, given the different nature of the parameter measured (i.e. hydrodynamic diameters vs. core-particle size), this procedure allowed to obtain a size estimation of CeO_2 NPs in good agreement with those obtained with different techniques (TEM, XRD and DLS).

The direct quantification of CeO_2 NPs by ICP-MS using the corresponding ionic standard led to low recoveries (<80%), similarly to those results reported in literature [46,47]. The alternative proposed in this work for quantifying CeO_2 NPs by FFFF-ICP-MS was the use of a CeO_2 NP suspension as cerium standard. The high sensitivity achieved with ICP-MS (LOD=0.9 μg L^{-1} CeO_2) converts the FFFF-ICP-MS tandem into an interesting alternative for studying CeO_2 NPs in environmental samples at low concentrations. Future work is envisioned for applying the different FFFF-ICP-MS methods for characterizing and quantifying synthetic CeO_2 NP on environmental samples related with the use of nanoceria-based diesel combustion catalysts.

Acknowledgements. This work was primarily supported by the Spanish Ministry of Economy and Competitiveness (MINECO) by funding the project CTQ2012-38091-C02-01. The author L.S-G. acknowledges a postdoctoral research grant co-funded by the *Fundación Agencia Aragonesa para la Investigación y Desarrollo de Aragón* (ARAID) and the *Institute of Environmental Sciences of Aragón* (IUCA), University of Zaragoza. The authors would like to acknowledge the use of *Servicio General de Apoyo a la Investigación*-SAI at Universidad de Zaragoza, and to thank Diamond Light Source for access to beamline I07 that contributed to the results presented here.

1. **References**European Commission, 2011/696/EU: Commission Recommendation of 18 October 2011 on the definition of nanomaterial, Off. J. Eur. Communities: Legis., 2011, 275, 38–40.
2. Gottschalk F, Nowack B. The release of engineered nanomaterials to the environment. J. Environ. Monit. 2011, 13: 1145-1155.
3. Sun CW, Li H, Chen LQ. Nanostructured ceria-based materials: synthesis, properties, and applications. Energy Environ. Sci. 2012, 8475-8505.
4. Mueller NC, Nowack B. Exposure modeling of engineered nanoparticles in the environment. Environ. Sci. Technnol. 2008, 42: 4447-4453.
5. Gottschalk F, Scholz RW, Nowack B. Probabilistic material flow modeling for assessing the environmental exposure to compounds: methodology and an application to engineered nano-TiO_2 particles. Environ. Model Softw. 2010, 25: 320-332.
6. Logothetidis S, Patsalas P, Charitidis C. Enhanced catalytic activity of nanostructured cerium oxide films. Mater. Sci. Eng. C 23 2003, 803-806.
7. Selvan VAM, Anand RB, Udayakumar M. Effects of cerium oxide nanoparticle addition in diesel and diesel–biodiesel–ethanol blends on the performance and emission characteristics of a CI engine. J. Eng. Appl. Sci., 2009, 4: 1–6.
8. O'Brien NJ, Cummins EJ. Ranking initial environmental and human health risk resulting from environmentally relevant nanomaterials. J. Environ. Sci. Health A. 2010, 45: 992–1007.

9. Johnson AC, Park B. Predicting contamination by the fuel additive cerium oxide engineered nanparticles within the United Kingdom and the associated risks. Environ. Toxicol. Chem. 2012, 31: 2582-2587.

10. Thill A, Zeyons O, Spalla O, Chauvat F, Rose J, Auffan M, Plank AM. Cytotoxicity of CeO_2 nanoparticles for Escherichia coli. Physico-chemical insight of the cytotoxicity mechanism. Environ. Sci. Technol. 2006, 40: 6151-6156.

11. Park B, Donaldson K, Duffin R, Tran L, Kelly F, Mudway I, Morin JP, Guest, R, Jenkinson P, Samaras Z, Giannouli M, Kouridis H, Martin P. Hazard and risk assessment of a nanoparticulate cerium oxide-based diesel fuel additive — a case study. Inhal. Toxicol. 2008, 20: 547–566.

12. Van Hoecke K, Quik JTK, Mankiewicz-Boczek J, Schamphelaere KAC, Elsaesser A, Van der Meeren P, Barnes C, McKerr G, Howard CV, Van de Meent D, Rydynski K, Dawson KA, Salvati A, Lesniak A, Lynch I, Silversmit G, de Samber B, Vincae L, Janssen CR. Fate and effects of CeO_2 nanoparticles in aquatic ecotoxicity tests. Environ. Sci. Technol. 2009, 43: 4537-4546.

13. Rogers NJ, Franklin NM, Apte SC, Batley GE, Angel BM, Lead JR, Baalousha M. physic-chemical behaviour and algal toxicity of nanoparticulate CeO_2 in freshwater. Environ. Chem. 2010, 7: 50-60.

14. Gaiser BK, Biswas A, Rosenkranz P, Jepson MA, Lead JR, Stone V, Tyler CR, Fernandes TF. Effects of silver and cerium dioxide micro- and nano-sized particles on Daphnia magna. J. Environ. Monitor. 2011, 13: 1227-1235.

15. Baalousha M, Ju-Nam Y, Cole PA, Gaiser B, Fernandes TF, Hriljac JA, Jepson MA, Stone V, Tyler CR, Lead JR. characterization of cerium oxide nanoparticles – Part 1: size measurements. Environ. Chem. 2012, 31: 983-993.
16. Saitzek S, Blach JF, Villain S, Gavarri JR. Nanostructured ceria: a comparative study from X-ray diffraction, Raman spectroscopy and BET specific surface measurements. Phys. Status Solidi 2008, 205:1534–1539.
17. Baalousha M, Stolpe B, Lead JR. Flow field-flow fractionation for the analysis and characterization of natural colloids and manufactured nanoparticles in environmental systems: A critical review. J. Chromatogr. A 2011, 1218: 4078-4103.
18. Thang NM, Geckeis H, Kim JI, Beck HP. Application of the flow field flow fractionation (FFFF) to the characterization of aquatic humic colloids: evaluation and optimization of the method. Colloid Surface A 2001, 101: 289-301.
19. Wahlund KG, Giddings JC. Properties of an asymmetrical flow field-flow fractionation channel having one permeable wall. Anal. Chem. 1987, 59: 1332-1339.
20. Taylor H, Garbarino JR. Inductively coupled plasma-mass spectrometry as an element-specific detector for field-flow fractionation particle separation. Anal. Chem. 1992, 64: 2036-2041.
21. Loeschner K, Navratilova J, Legros S, Wagner S, Grombe R, Snell J, Kammer F, Larsen EH. Optimization and evaluation of asymmetric flow field-flow fractionation of silver nanoparticles. J. Chromatogr. A 2013, 1272: 116-125.
22. Heroult J, Nischwitz V, Bartczak D, Goenaga-Infante H. The potential of asymmetric flow field-flow fractionation hyphenated to multiple detectors for the quantification and

size estimation of silica nanoparticles in a food matrix. Anal. Bioanal. Chem. 2014, 406: 3919–3927.

23. Bouby M, Geckeis H, Manh TN, Yun JI, Dardenne K, Schafer T, Walther C, Kim JI, Laser-induced breakdown detection combined with asymmetrical flow field-flow fractionation: application to iron oxi/hydroxide colloid characterization. J. Chromatogr. A. 2004, 1040: 97-104.
24. Baalousha M, Kammer FVD, Motelica-Heino, Baborowski M, Hofmeister C, Le Coustumer P. Size-based speciation of natural colloidal particles by flow field flow fractionation, inductively coupled plasma-mass spectroscopy, and transmission electron microscopy/X-ray energy dispersive spectroscopy: colloids-trace element interaction. Environ. Sci. Technol. 2006, 40: 2156-2162.
25. Bolea E, Laborda F, Castillo JR. Metal associations to microparticles, nanocolloids and macromolecules in compost leachates: size characterization by asymmetrical flow field-flow fractionation coupled to ICP-MS. Anal. Chim. Acta. 2010, 661: 206-214.
26. Barahona F., Geiss O, Urbán P., Ojea-Jiménez I, Gilliland D., Barrero-Moreno J. Simultaneous determination of size and quantification of silica nanoparticles by Asymmetric Flow Field-Flow Fractionation coupled to ICPMS using silica nanoparticles standards. Anal. Chem. 2015, 87: 3039-3047.
27. Bolea E, Jiménez-Lamana J, Laborda F, Castillo JR. Size characterization and quantification of silver nanoparticles by asymmetric flow filed-flow fractionation coupled with inductively coupled plasma mass spectrometry. Anal. Bioanal. Chem. 2011, 401: 2723-2732.

28. Cornelis G, Ryan B, McLaughlin MJ, Kirby JK, Beak D, Chittleborough D. Solubility and batch retention of CeO_2 nanoparticles in soils. Environ. Sci. Technol. 2011, 45: 2777–2782.

29. Keller AA, Wang H, Zhou D, Cardinale BJ, Miller R, Ji Z. Stability and aggregation of metal oxide nanoparticles in natural aqueous matrices. Environ. Sci. Technol. 2010, 44: 1962-1967.

30. Limbach LK, Bereiter R, Müller E, Krebs R, Gälli R, Stark W.J. Removal of oxide nanoparticles in a model wastewater treatment plant: influence of agglomeration and surfactants on clearing efficiency. Environ. Sci. Technol. 2008, 42: 5828–5833.

31. Susanto H, Ulbricht M. Characteristics, performance and stability of polyethersulfone ultrafiltration membranes prepared by phase separation method using different macromolecular additives. J. Membr. Sci. 2009, 327: 125–135.

32. Cumberland SA, Lead JR. Particle size distributions of silver nanoparticles at environmentally relevant conditions. J. Chromatogr. A. 2009, 1216: 9099–9105.

33. Schimpf ME, Caldwell K, Giddings JC. Field-flow fractionation handbook. John Wiley and Sons (USA). 2000, 616 p.

34. Litzen A, Wahlund KG. Zone broadening and dilution in rectangular and trapezoidal asymmetrical flow field-flow fractionation channels. Anal. Chem 1991, 63: 1001–1007.

35. MacCuspie RI, Rogers K, Patra M, Suo Z, Allen AJ, Martin MN Hackley VA. Challenges for physical characterization of silver nanoparticles under pristine and environmentally relevant conditions. J. Environ. Monit. 2011, 13: 1212–1226.

36. Cepriá G, Córdova WR, Céspedes O, Sánchez-García L, Ferrer P, Gianolio D, Castillo JR. Structure, size and redox properties of cerium (IV) oxide nanoparticles. Nanotechnology 2015 (submitted).
37. Filella, M.; Zhang, J. W.; Newman, M. E.; Buffle, J. Colloids Surf. A. 1997, 120: 27–46.
38. Bouby M, Geckeis H, Geyer FW. Application of asymmetric flow field-flow fractionation (AsFlFFF) coupled to inductively coupled plasma mass spectrometry (ICPMS) to the quantitative characterization of natural colloids and synthetic nanoparticles. Anal. Bioanal. Chem. 2008, 392: 1447–1457.
39. Dubascoux S, Le Hécho I, Potin Gautier M, Lespes G. Online and off-line quantification of trace elements associated to colloids by As-Fl-FFF and ICP-MS. Talanta 2008, 77: 60–65.
40. Wagner S, Legros S, Loeschner K, Liu J, Navratilova J, Grombe R, Linsinger TPJ, Larsen EH, von der Kammer F, Hofmann T. First steps towards a generic sample preparation scheme for inorganic engineered nanoparticles in a complex matrix for detection, characterization, and quantification by asymmetric flow-field flow fractionation coupled to multi-angle light scattering and ICP-MS. J. Anal. At. Spectrom. 2015, 30: 1286-1296.
41. Hoque ME, Khosravi K, Newman K, Metcalfe CD. Detection and characterization of silver nanoparticles in aqueous matrices using asymmetric-flow field flow fractionation with inductively coupled plasma mass spectrometry. J. Chromat. A. 2012, 1233: 109-115.

42. Gigault J, Hackley VA. Observation of size-independent effects in nanoparticle retention behaviour during asymmetric-flow field-flow fractionation. Anal. Bioanal. Chem. 2013, 405: 6251-6258.

43. Giddings JC. Factors influencing accuracy of colloidal and macromolecular properties measured by field-flow fractionation. Anal. Chem. 1997, 69: 552-557.

44. Bolea E, Jiménez-Lamana J, Laborda F, Abad-Álvaro I, Arola L, Castillo JR. Detection and characterization of silver nanoparticles and dissolver species in culture medium and cells by AsFlFFF-UV-Vis-ICPMS: Application to nanotoxicity tests. Analyst 2014, 139: 914-922.

45. Aureli F, D'Amato M, Raggi A, Cubadda F. Quantitative characterization of silica nanoparticles by asymmetric flow field flow fractionation coupled with online multiangle light scattering and ICP-MS/MS detection. J. Anal. At. Spectrom. 2015, 30: 1266-1273.

46. Fabricius A-L, Duester L, Meermann B, Ternes TA. ICP-MS-based characterization of inorganic nanoparticles-sample preparation and off-line fractionation strategies. Anal. Bioanal. Chem. 2014, 406: 467-479.

47. Motellier S, Guiot A, Legros S, Fiorentino B. Elemental recoveries for metal oxide nanoparticles analysed by direct injection ICP-MS: influence of particle size, agglomeration state and sample matrix. J. Anal. At. Spectrom. 2014, 29: 2294-2301.

48. Hassellöv, M., Lyvén, B., Haraldsson, C., & Sirinawin, W. (1999). Determination of continuous size and trace element distribution of colloidal material in natural water by on-line coupling of flow field-flow fractionation with ICPMS. Analytical Chemistry, 71(16), 3497–3502.

Table 1. Optimal conditions for the Asymmetric Flow-Field Flow Fractionation separations.

	Time (min)		Flow rate (mL min^{-1})
Spacer		190 or 350 μm	
Membrane		PES (5 KDa)	
Injection	4		0.20
Transition	1		
Initial Crossflow			1.0
Crossflow Program	25	Constant	0.325
	5	Linear decay	0.325 to 0
	5	Constant	0
Total	40		
Detector flow			1.0
Carrier	0.05 % SDS pH 10		

Table 2. Optimal conditions for the Hollow Fiber-Field Flow Fractionation separations.

	Time (min)		Flow rate (mL min^{-1})
Injection	4		0.20
Transition	1		
Initial Crossflow			0.05
Crossflow Program	30	Constant	0.05
	2	Linear decay	0.05 to 0
	3	Constant	0
Total	40		
Detector flow			1.0
Carrier	0.05 % SDS pH 10		

Table 3. Recovery values (%) of the CeO_2 NPs in standards STD-4 (4 nm) and STD-10 (10-20 nm) with the two FFFF methods (AF4[a] and HF5[b]) and different mobile phase composition. The results derived from absorbance signals at the maximum wavelength are expressed as mean ± standard deviation (n=3). AF4 Polyether sulfone (PES) membrane 5 kDa cutoff. HF5 fiber cartridge of 10 KDa PES membrane.

		STD-4				STD-10			
		0.01 % SDS	0.05 % SDS	0.1 % SDS	0.05 % Novachem	0.01 % SDS	0.05 % SDS	0.1 % SDS	0.05 % Novachem
AF4	Spacer 190 µm	23±8	72±3	18±5	101±2	67±12	77±9	67±3	100±2
	Spacer 350 µm	-	75±1	-	-	-	83±2	-	-
HF5		-	90±10	-	-	-	94±2	-	-

[a] Asymmetric Flow-Field Flow Fractionation.
[b] Hollow Fiber-Field Flow Fractionation.

Table 4. Multi-method determination of CeO_2 NP size (nm) in STD-4, STD-10, and a commercial suspension as physical (core particle) or hydrodynamic diameter. Nominal sizes reported by manufacturer are also included.

	STD-4 (nm)	STD-10 (nm)	Commercial suspension (nm)
nominal	4	10-20	30[a]
TEM[b]	3 (1-5)	4 (1-10)	2-65
XRD[c]	2	5	40
DLS[d] (HNO_3 0.01M) (polydispersity)[e]	5 (0.133)	8 (0.071)	26 (0.173)

[a] Determined by BET.

[b] Size reported as the number-based size distribution observed from the frequency histogram (Fig. 3). In parenthesis the size range of the histogram. For the commercial suspension, no histogram was obtained, and size is reported as a range of values, given the large heterogeneity in shape and size observed (Fig. S3).

[c] Average crystalline particle size (section S4 in Supplementary Information).

[d] Hydrodynamic diameter (section S2 in Supplementary Information).

[e] Values <0.1 attributed to monodisperse samples, between 0.1 and 0.3 to polydisperse samples.

Table 5. Estimation of CeO_2 NP size (nm) in STD-10 and a commercial suspension by FFFF using different calibration strategies and different configurations; *w* is the experimentally determined channel thickness, *a* and *b* are the y-intercept and slope empirically determined for each calibration configuration. Results are expressed as size estimated from the peak maximum ±uncertainty from mass-size distributions derived from fractograms.

AF4	*w* (μm)	*a*	*b*	Calibration strategy	STD-10 (nm)	Commercial suspension (nm)
Spacer: 350 μm	313	-	-	based on theory, using azide	16±8	47±20
	189	-	-	based on theory, using NIST Au NPs	29±14	81±35
	-	-0.3808	0.2859	vs Ag NPs standards	36±20	n.m.
	-	-0.4091	0.2324	vs SiO_2 NPs standards	16±11	65±40
Spacer: 190 μm	-	-0.0658	0.0151	vs SiO_2 NPs standards	21±14	52±32
HF5	-	-0.2812	0.1593	vs SiO_2 NPs standards	20±16	57±37

Conditions listed in table 1 (AF4) and 2 (HF5). n.m. stands for not measured.

Table 6. Recoveries of cerium measured in STD-4, STD-10 and a commercial suspension by ICP-MS direct nebulization using Ce(IV) or CeO_2 NPs as concentration standards (mean±standard deviation; n=5). Quantification of CeO_2 NPs in the commercial suspension by direct nebulization in ICP-MS, by using STD-10 as quantification standard. FFFF system used: AF4 with a 350 μm. Separation conditions listed in table 1.

	ICP-MS recovery (%)[a]		AF4-ICP-MS recovery (%)	Channel recovery (%)[b]	Corrected AF4-ICP-MS recovery (%)
	vs Ce(IV) std	vs CeO_2–NPs std	vs CeO_2–NPs std		vs CeO_2–NPs std
STD 4	58±4	-	-	-	-
STD-10	62±6	-	-	-	-
Commercial suspension	73±7	97±7	81±3	82±9	99±9

[a] Relative to concentration measured after microwave-assisted acid digestion.
[b] Mass recovered from AF4 channel.

Figure captions:

Fig. 1. Zeta potential values of the two CeO_2-NP standards (STD-4 and STD-10) and a commercial suspension in the pH range 2-11.

Fig. 2. Effects of mobile phase composition (at pH 10) on the peak shape of the STD-4 CeO_2 NPs: a) 0.01 % SDS; b) 0.05% SDS; c) 0.05% mixed surfactant Novachem. Measurements on AF4 with spacer of 190 μm.

Fig. 3. Transmission Electron Microscopy (TEM) images and histograms of size distributions in number of CeO_2 NPs in STD-4 (a,b) and STD-10 (c,d). Images obtained by applying bright field (b) or high angle annular dark filter (d) techniques. Scale bars 10 nm or 20 nm (b and d, respectively).

Fig. 4. Comparison of the resolution and peak shape of STD-4 (full line) and STD-10 (dashed line) with AF4: a) spacer 190 μm and b) 350 μm, and with HF5 (c). Optimal separation conditions used (tables 1 and 2).

Fig. 5. Transmission Electron Microscopy (TEM) images of the CeO_2 NPs in the commercial suspension, with high angle annular dark filter (a, b) and bright field (c) techniques. Scale bars are 100 nm (a), 50 nm (b), and 10 nm (c). No size histogram could

be made in this sample due to the large heterogeneity in shape and size of the NPs in the commercial suspension.

Fig. 6. Mass-size distribution of CeO_2 NPs in the commercial suspension, derived from applying the FFFF theory. AF4-ICP-MS with a 350 μm spacer. Experimental conditions listed in Table 1.

FIGURE 1

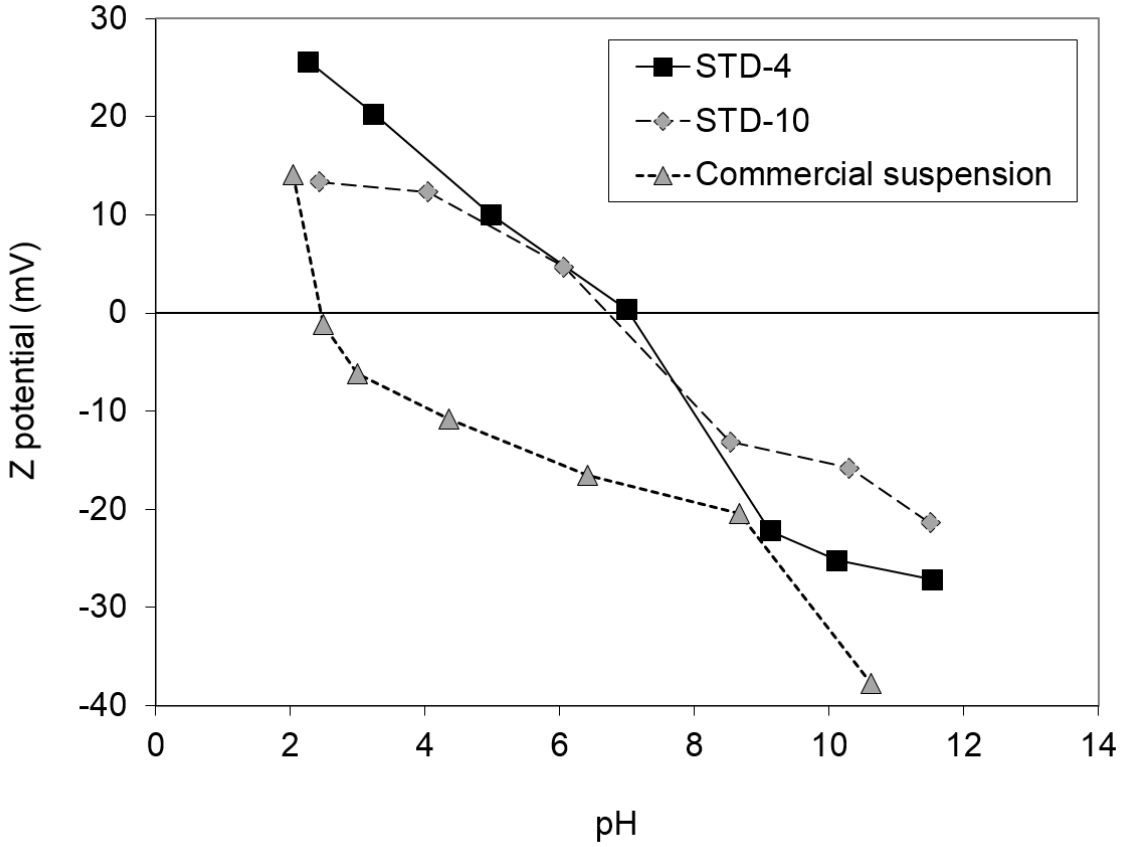
30
20
10
0
-10
-20
-30
-40
Z potential (mV)
0
2
4
6
8
10
12
14
pH
STD-4
STD-10
Commercial suspension

FIGURE 2

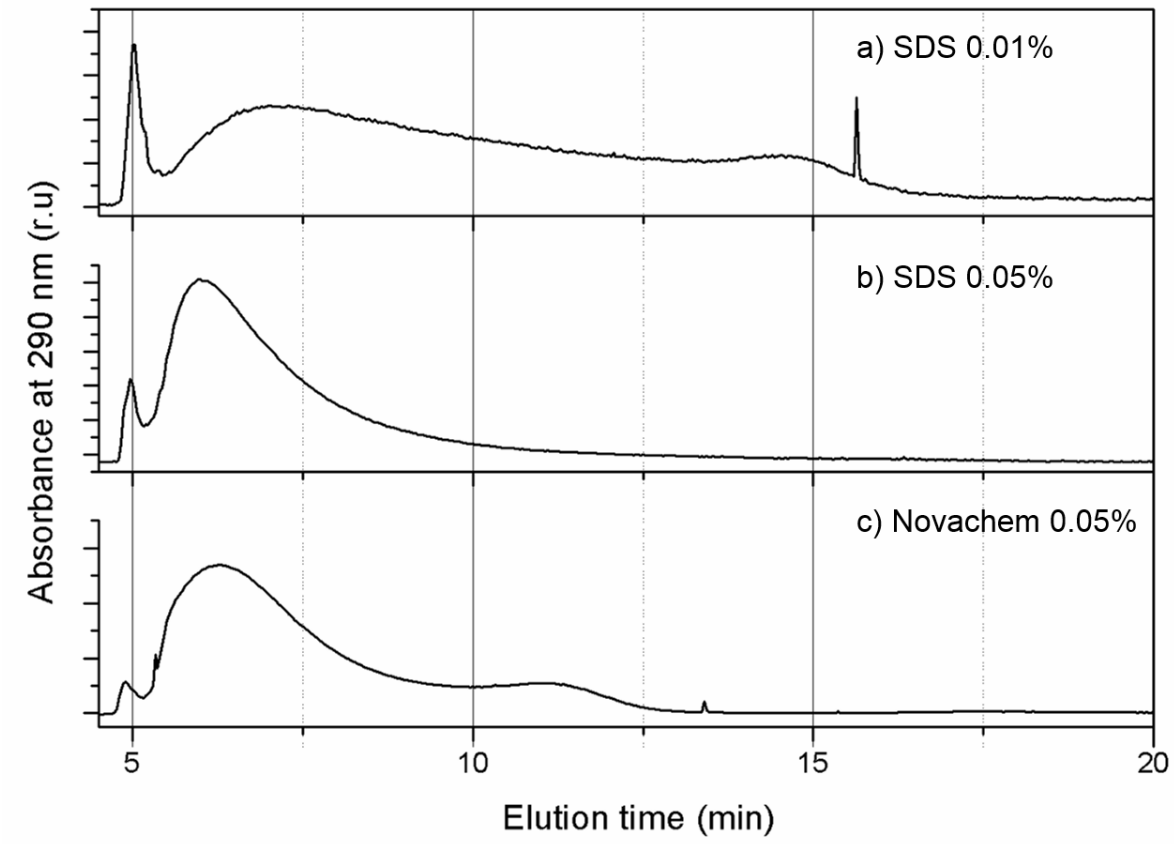
a) SDS 0.01%
b) SDS 0.05%
c) Novachem 0.05%
Absorbance at 290 nm (r.u)
5
10
15
20
Elution time (min)

FIGURE 3

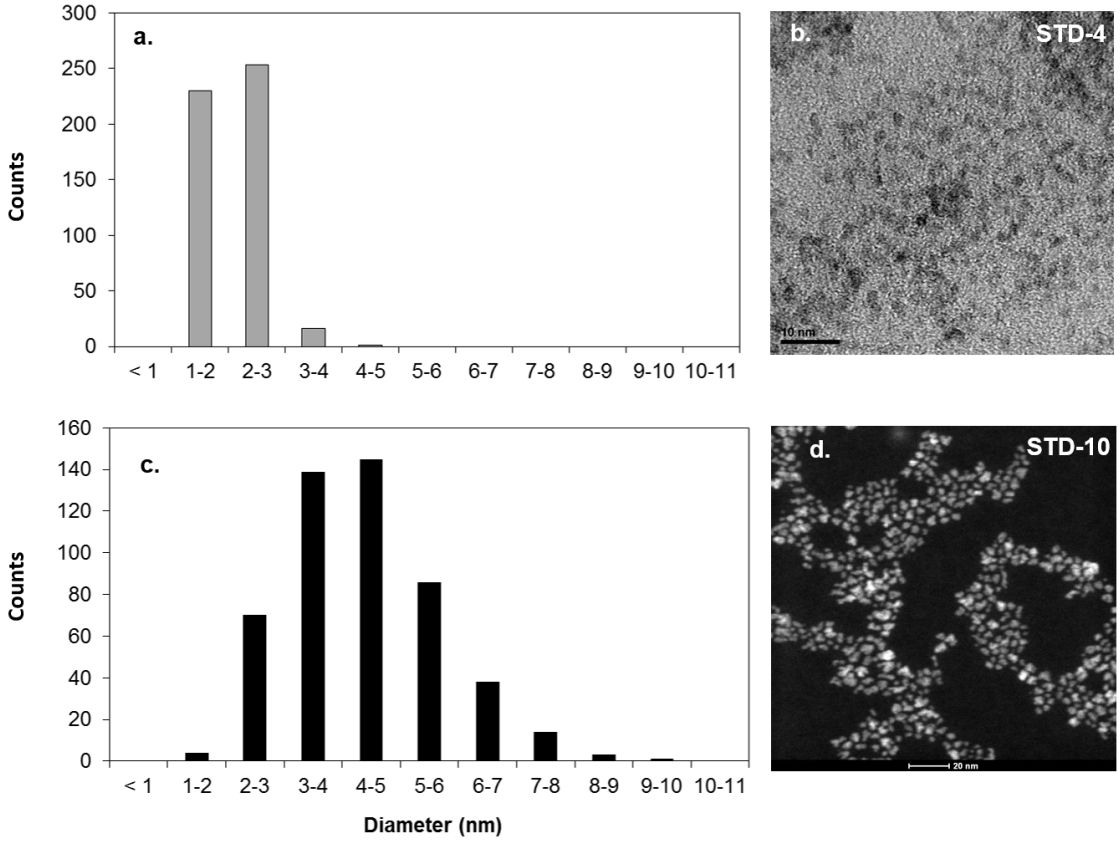
a.
Counts
300
250
200
150
100
50
0
< 1
1-2
2-3
3-4
4-5
5-6
6-7
7-8
8-9
9-10
10-11
b.
STD-4
10 nm
c.
Counts
160
140
120
100
80
60
40
20
0
Diameter (nm)
d.
STD-10
20 nm

FIGURE 4

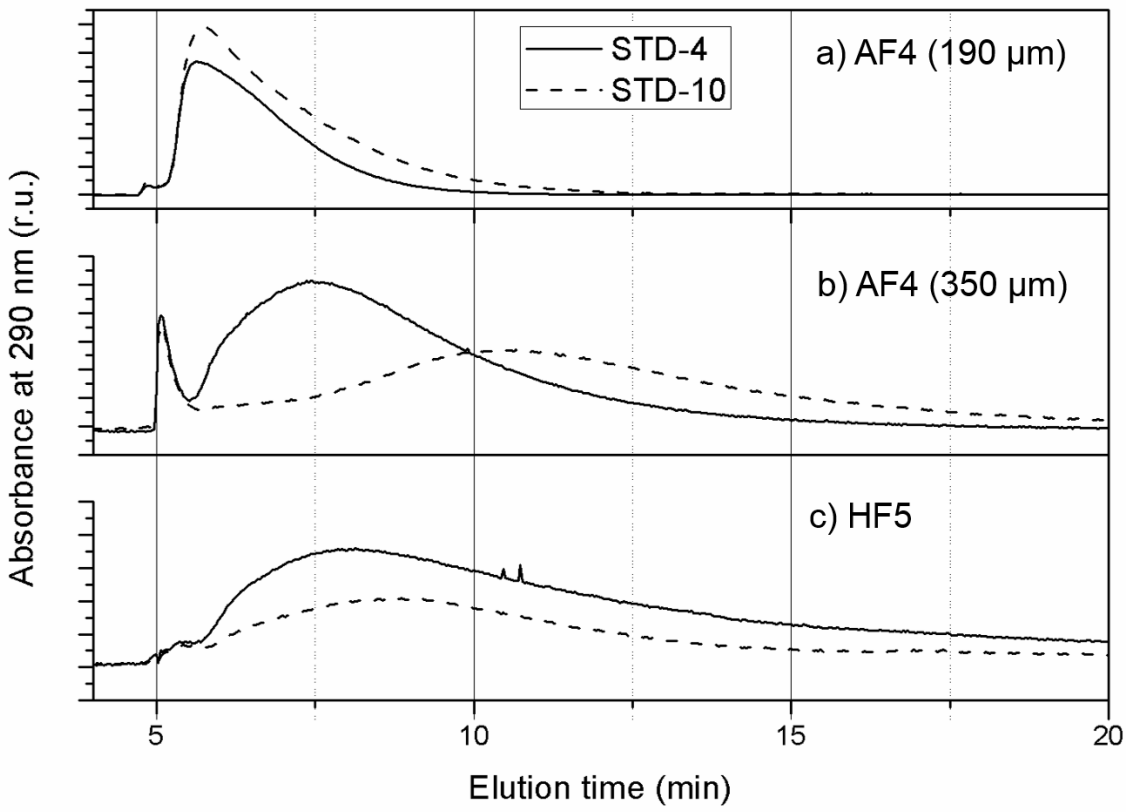
STD-4
STD-10
a) AF4 (190 µm)
b) AF4 (350 µm)
c) HF5
Absorbance at 290 nm (r.u.)
5
10
15
20
Elution time (min)

FIGURE 5

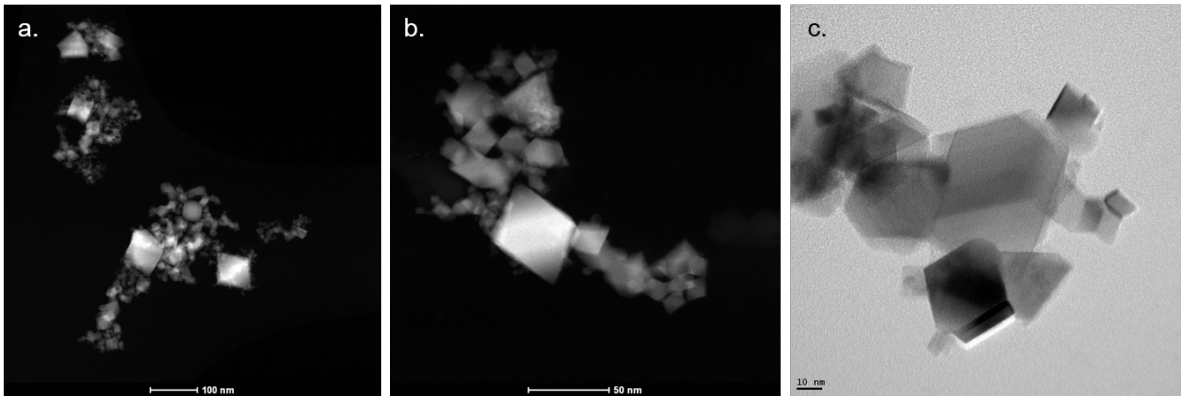

FIGURE 6

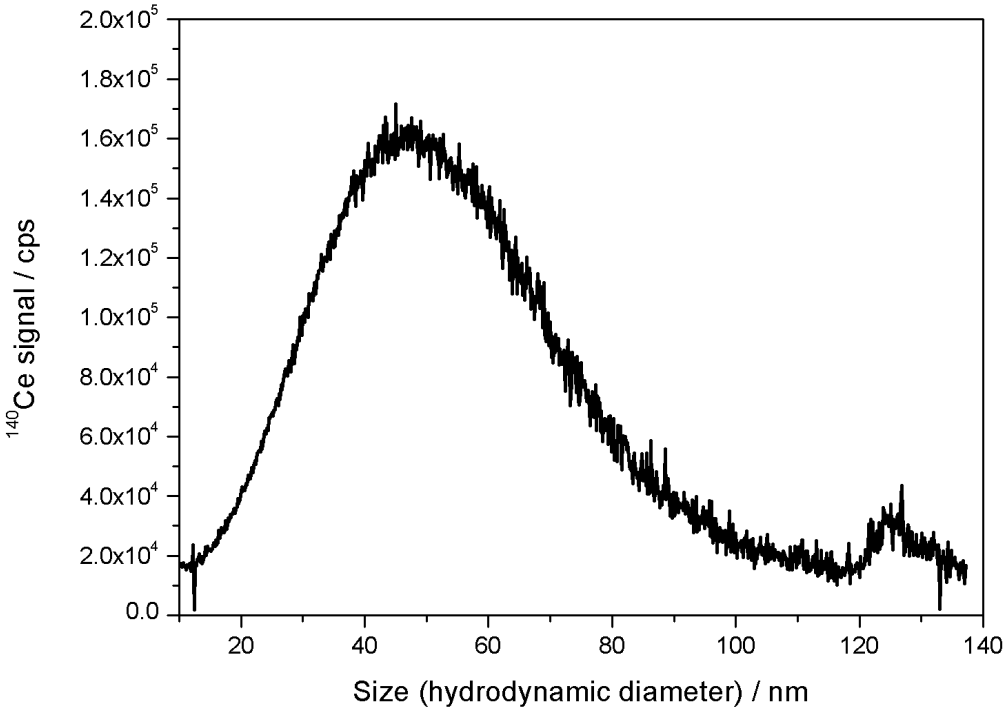
2.0x10^5
1.8x10^5
1.6x10^5
1.4x10^5
1.2x10^5
1.0x10^5
8.0x10^4
6.0x10^4
4.0x10^4
2.0x10^4
0.0
140Ce signal / cps
20
40
60
80
100
120
140
Size (hydrodynamic diameter) / nm

Supplementary Information

Size determination and quantification of engineered cerium oxide nanoparticles by flow field-flow fractionation coupled to inductively coupled plasma mass spectrometry

L. Sánchez-García[1], E. Bolea[1], F. Laborda[1], C. Cubel[1], P. Ferrer[2], Diego Gianolio[2], I. da Silva[3], J.R. Castillo[1].

[1] Group of Analytical Spectroscopy and Sensors (GEAS). Institute of Environmental Sciences (IUCA). University of Zaragoza, Pedro Cerbuna 12, 50009 Zaragoza, Spain.
[2] Diamond Light Source, Harwell Science and Innovation Campus, Chilton, Didcot OX11 0DE, UK.
[3] ISIS Facility, Rutherford Appleton Laboratory, Chilton, Oxfordshire OX11 0QX, UK.

S.1. The FFFF theory and its application to particle size calibration:

The retention of an analyte component is quantified by its retention ratio R, defined as the component's velocity through the channel relative to the average velocity of the carrier liquid. Experimentally, the retention ratio is calculated as the ratio $R = t_o/t_r$, where t_0 is the elution time of void peak and t_r the elution time of the analyte. Under the action of a cross-flow field, the individual species injected into the channel are present at a certain average distance *l* from the accumulation wall:

$$l = D/u \quad (1)$$

where D is the diffusion coefficient in the carrier and *u* the induced field flow. Instead of *l*, the dimensionless retention parameter λ can be used [1]:

$$\lambda = l/w \quad (2)$$

where *w* corresponds to the channel width or thickness.

In FFFF, where the crossflow is constant throughout the channel, λ is a constant defined for each analyte by [2]:

$$\lambda = V_0 D / V_c w^2 \quad (3)$$

where V_0 is the geometric volume of the channel and V_c is the crossflow rate. For highly retained species ($\lambda < 0.02$), the retention parameter can be related to the retention ratio by the following expression [3]:

$$R \cong 6\lambda \quad (4)$$

Therefore, FFFF allows the determination of the diffusion coefficient D and according to the Stokes equation:

$$d_h = kT / 3\pi\eta D \quad (5)$$

where d_h is the hydrodynamic diameter, k is the Boltzmann constant, T is the temperature, and η is the viscosity of the carrier. The hydrodynamic diameter d_h is accessible without any calibration as follows:

$$R = 2V_0 kT / \pi\eta d_h V_c w^2 \quad (6)$$

The use of the FFFF theory allow to obtain information about the size of the eluted species, by using the abovementioned theoretical equations. This requires the measurement of the experimental channel width (w), which in this study was obtained by means of two different approaches, measuring (1) the elution time of an unretained substance, or (2) the retention time of a substance of known diffusion coefficient.

In the first approach, sodium azide was injected as a non-retainable species into the AF4 and its elution time with and without using channel was measured (n=4 each). A loop of 100 µl and the following conditions were employed: tip flow rate of 0.5 mL min^{-1}, crossflow rate (V_c) of 0.01 mL min^{-1}, and flow rate out of the channel (V_{out}) of 0.49 mL min^{-1}, when operating with channel, and tip flow of 0.5 mL min^{-1} without V_c and V_{out} , when operating without channel. The connections volume (mL) was calculated by using V_{out} (mL min^{-1}) and the mean elution times estimated with and without the channel (min). The width of the spacer

was then estimated for a specific area of the channel (32.7 cm^2), and the empirical width of the channel (*w*) derived from subtracting the width values obtained from operating with and without channel.

In the second approach, the retention ratio (R) of Au NPs of 60 nm from NIST (Gaithersburg, USA) was used to calculate λ and thereby to resolve *w*. For that, the TEM-empirical diameter of Au NP was used (i.e. 56 ± 0.5 nm).

S.2. Dynamic Light Scattering (DLS)

DLS measurements were conducted with a Brookhaven 90Plus DLS instrument (Brookhaven Instruments, Holtsville, NY, USA) in disposable plastic cuvettes, and the mean of five measurements was taken. The effective diameter in a particle distribution is measured as an average diameter weighted by the intensity of the light scattered by each particle. In this study, the intensity weighting was done averaging the number of NPs, given the polydispersity of the suspensions studied.

Table S1. Influence of ionic strength on the recovery (%) of the CeO_2-NPs standards in AF4. The results derived from absorbance signals at the maximum wavelength are expressed as mean ± standard deviation (n=3). Polyether sulfone membrane 5 kDa cutoff.

Mobile phase composition		STD-4
SDS	0.05%	72±3
SDS	0.05% (1 mM $NaNO_3$)	60±5
SDS	0.05% (5 mM $NaNO_3$)	61±4

S.3. Study of separation conditions.

The study of the effects of separation conditions on the resolution of fractograms peaks was based on the analysis of the peak width and retention time. The simplified expressions used here for discussing the peaks retention time (t_r) and width (σ_t) are derived from the flow FFF theory, on the basis of experimental variables [4] and the standard deviation of a peak of a monodisperse compound retained [5], respectively:

$$t_r = w^2/6D_i \cdot ln(1+V_c/V_{out}) \quad (7)$$

Where w is the thickness of the spacer, D_i is the substance diffusion coefficient, V_c is the crossflow rate, and V_{out} the flow rate out of the channel. For a given substance and fixed w (here 190 μm), t_r depends on the V_c/V_{out} ratio, where higher V_c leads to longer retention times.

$$\sigma_t = 0.82 \cdot A_w/V_c \cdot [\ln(1+V_c/V_{out})]^{1/2} \quad (8)$$

Where A is the area of the porous channel wall. For a given V_c/V_{out} ratio, the highest crossflow rate has to be applied to obtain peaks as narrow as possible [6].

Resolution of two studied peaks is calculated according to the expression:

$$R_S = 1.176\ [(t_{r2}-t_{r1})/(w_1^{0.5}+w_2^{0.5})] \quad (9)$$

where t_{ri} is the retention time of peak i, and $w_i^{0.5}$ is the width of the peak i at half height.

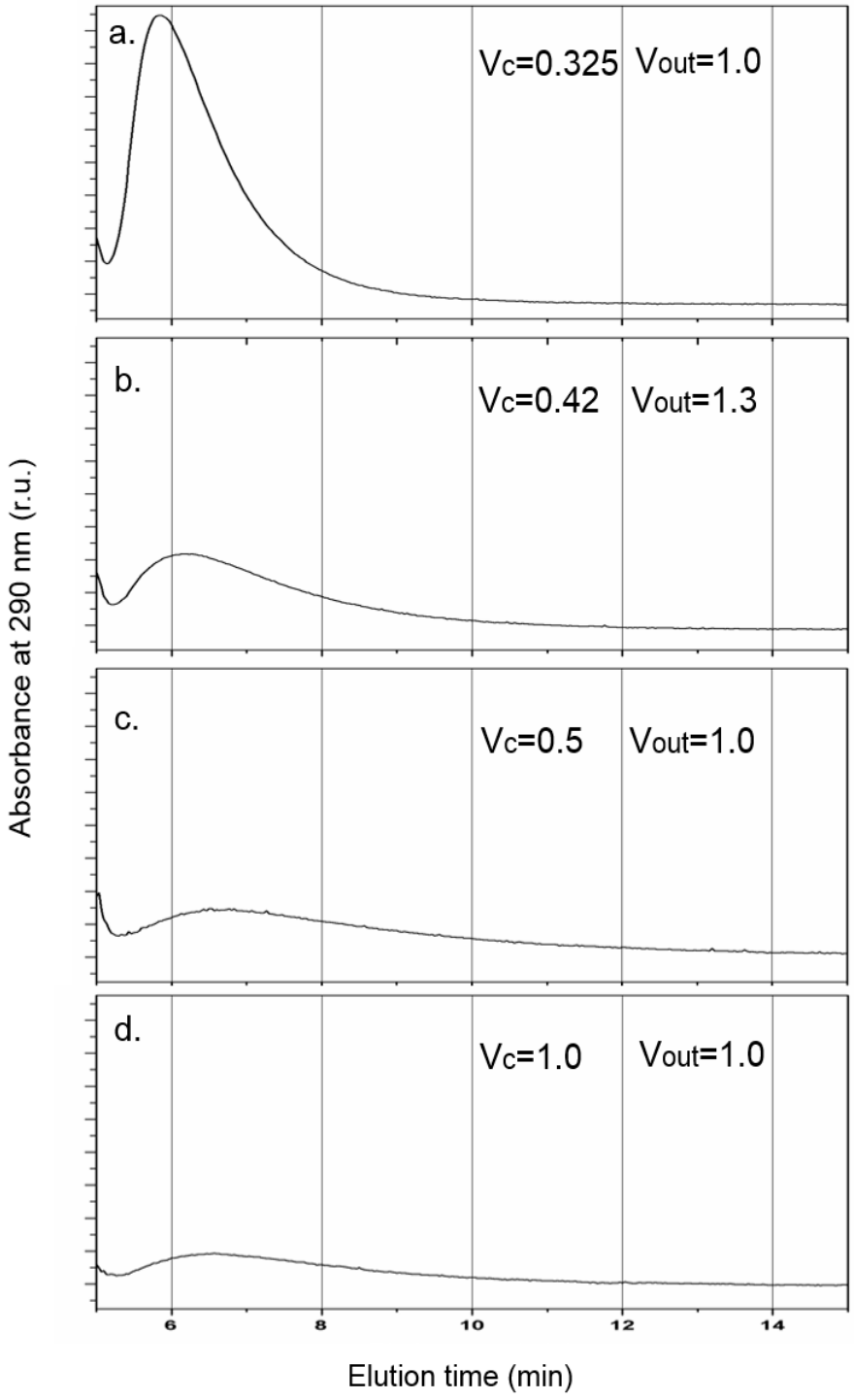

Figure S1. Effect of crossflow (V_c) and outflow (V_{out}) on the elution of CeO_2 NP (STD-4) in AF4, at V_c/V_{out} ratios of 0.325 (a, b), 0.5 (c) and 1.0 (d). Mobile phase 0.05% SDS at pH 10.

S.4. X-ray powder diffraction (XRD):

X-ray powder diffraction (XRD) is a non-destructive technique that can provide with atomic structural information from crystalline samples, as well as information about the crystalline domain sizes of the compound studied. Therefore, this technique can be used to quantify the nanoparticle size of the samples [7].

The XRD patterns were collected on the I07 beamline at Diamond Light Source (UK), using a fixed wavelength of 0.866 Å and at room temperature. Small subaliquots of the STD4, STD10 and commercial product suspensions were deposited on a flat surface to evaporate the solvents at room temperature for three days and the remaining powder was then milled on an agate mortar pestle. Diffraction pattern measurements were carried out in a 2θ-step scan mode. Data was collected in the 2θ range of 9–50°, which corresponds to a d-space resolution of about 0.8 Å. Refinement of diffraction patterns was carried out by means of the Rietveld method [8], using Topas-Academic V5 program [9].

Results from the refinement of diffraction patterns show that only diffraction intensity coming from CeO_2 compound was found on all the samples measurements (Fig. S2).

In order to estimate the average crystalline particle size for each sample, a line-broadening study of the diffraction peaks [10] was performed on each dataset. Results obtained are shown in Table S2. STD-4 and STD-10 diffraction patterns were refined with a single CeO_2 phase, showing a NPs size of 2 and 5 nm, respectively. However, best fit obtained for the commercial product sample was achieved by using two CeO_2 phases with different lattice parameter, but same average particle size of 40 nm. The CeO_2 structure with a = 5.390 Å represents the 75% of the sample, while the one with a = 5.405Å accounts for a 25%. The CeO_2 theoretical lattice parameter is 5.406 Å (ISCD number 290464), which is bigger than the contracted lattice obtained for the NPs.

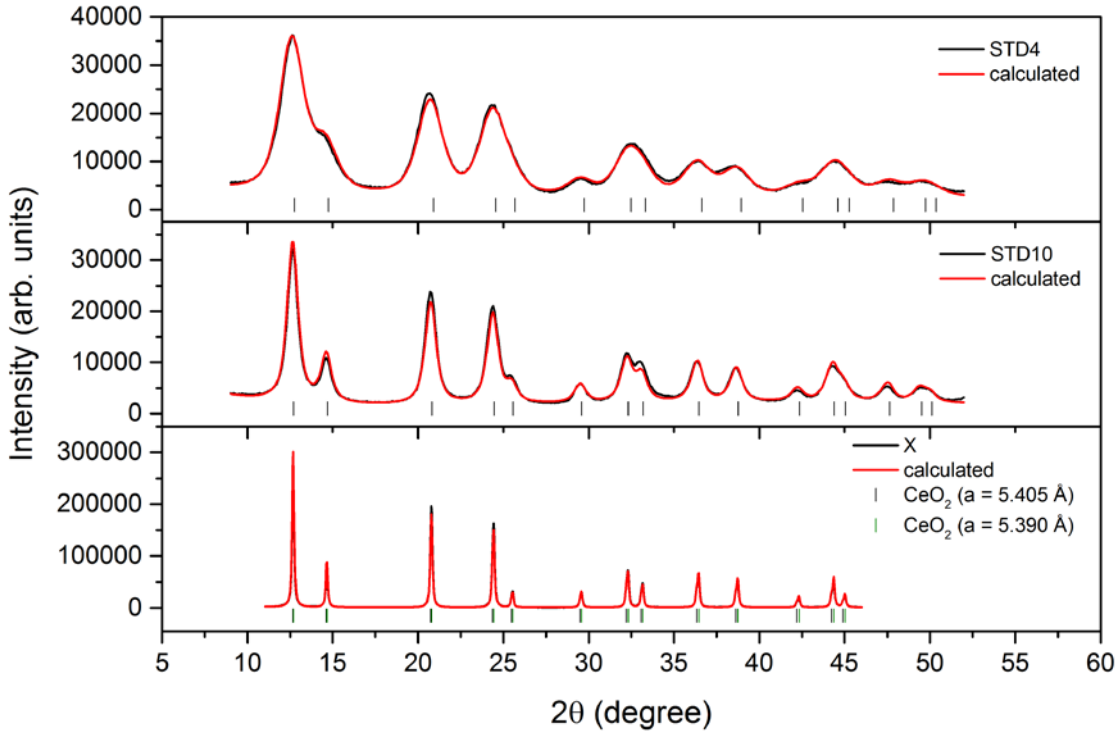

Figure S2. Experimental (black) and calculated by Rietveld method (red) XRD pattern for STD-4, STD-10 and commercial suspension (X). Allowed CeO_2 reflection positions are indicated by vertical lines, below each pattern.

Table S2. Average nanoparticle size and cubic lattice parameters obtained from the refinement of diffraction patterns of STD-4, STD-10 and the commercial suspension.

Sample	Average particle size (nm)	Lattice parameters (Å)
STD-4	2	5.360
STD-10	5	5.384
Commercial suspension	40	5.390 5.405

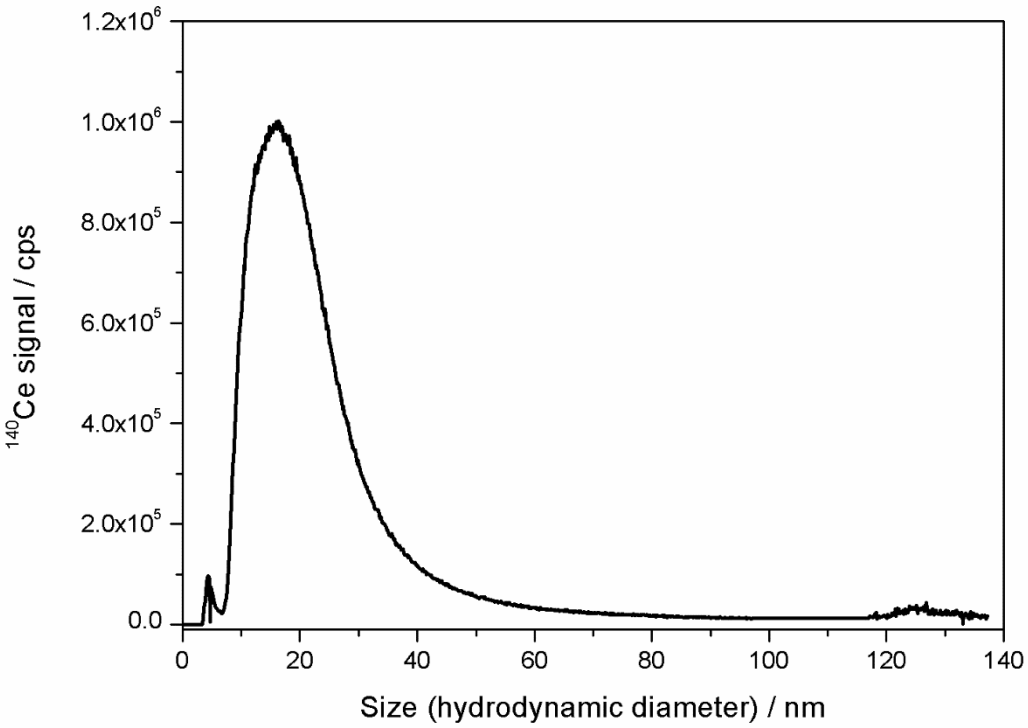

Figure S3. Mass-size distribution of CeO_2 NPs in the STD-10, derived from applying the FFFF theory. AF4-ICP-MS with a 350 μm spacer. Experimental conditions listed in Table 1.

S.5. X-ray Absorption Spectroscopy (XAS)

X-ray Absorption Spectroscopy (XAS) is a technique that provides geometrical and electronic information related with the type of neighboring atoms, structure and the density of materials. The number of atoms in the first coordination sphere correlates well with the packing level of the atoms and NP sizes [11]. In this study, XAS was focused on the EXAFS region (Extended X-ray Absorption Fine Structure), where the level of the atom packing and geometric arrangement of atoms on the coordination number(s) can be correlated with the NPs size. In CeO_2 NPs, each Ce is surrounded by 8 atoms, but the coordination sphere for the Ce ion located on the surface of the NP is formed by fewer atoms, so the packing level of Ce in large CeO_2 NPs is higher than for the small ones. NPs of different sizes show a different

surface-to-bulk ratio (determined as a ratio of fully coordinated: non-fully coordinated atoms in the cluster), which influences the average coordination number probed by EXAFS. Thus it is possible to reverse the problem and try to estimate the NP size from the intensity of the FT of the EXAFS signal which reflects the radial distribution function centred on the absorbing atom. XAS measurements were performed at room temperature on the B18 beamline at Diamond Light Source (UK) [12]. Data were collected at Ce-L_3 edge (E = 5726 eV) in CeO_2 NPs in the fluorescence yield mode with a 9-element Germanium detector using a double crystal Si(111) monochromator and Pt-coated branch. Harmonics were rejected with a pair of harmonic rejection mirrors. The energy was scanned from 5526 to 6156 eV (ca.10.5 $Å^{-1}$ in k-space) in 0.5 eV step interval. The Ce-Lα_1 fluorescence line was recorded with the detector placed parallel to the X-ray electric polarization field (i.e. forming 90º from the incoming X-ray beam). Data treatment was achieved with ATHENA software [13].

Although specific size estimations could not be derived from XAS, the analysis of the EXAFS region provided semi-quantitative information of the CeO_2-NPs size in the standards (STD-4 and STD-10) relative to the commercial suspension. Considering that the intensity of the signal around the first coordination sphere (maximum centered at 1.85Å in the phase–uncorrected FT EXAFS; Fig. S4) is related with the packing level of the Ce, relative information about the NP size can be obtained. The greater EXAFS signal observed for product X indicates that it shows a higher packing level, and thus larger CeO_2 NPs than those in STD-4 and STD-10.

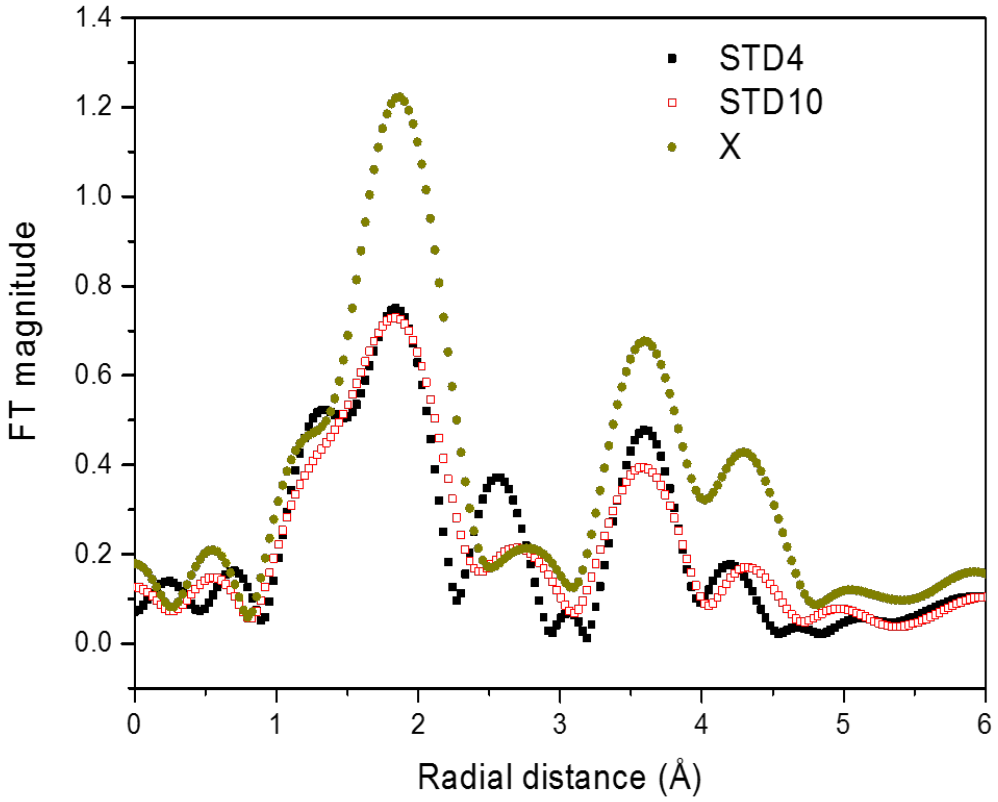

Figure S4. Radial distribution function of the CeO_2 NP standards (STD-4 and STD-10) and the commercial suspension (X), derived from the XAS analysis of the Extended X-ray Absorption Fine Structure (EXAFS). The FT EXAFS signal around the first coordination sphere (maximum centred at 1.85 Å) corresponds to the Ce-O bond length of 2.24 Å in real space and relates with the NP size.

References

1. Thang NM, Geckeis H, Kim JI, Beck HP. Application of the flow field flow fractionation (FFFF) to the characterization of aquatic humic colloids: evaluation and optimization of the method. Colloid Surface A 2001, 101: 289-301.
2. Schimpf ME, Caldwell K, Giddings JC. Field-flow fractionation handbook (Eds. ME Schimpf, K Caldwell and JC Giddings). John Wiley and Sons. (USA). 2000, 616 p.
3. Hassellov M, von der Kammer F, Beckett R. Characterization of aquatic colloids and macromolecules by Field-Flow Fractionation. In: Wilkinson KJ, Leads JR (Eds.), Environmental colloids and particles: behavior, separation and characterization. IUPAC Series on Analytical and Physical Chemistry of Environmental Systems 2006. Vol. 10. Wiley & Sons, pp. 224-276.
4. Wahlund KG, Giddings JC. Properties of an asymmetrical flow field-flow fractionation channel having one permeable wall. Anal. Chem. 1987, 59: 1332-1339.
5. Litzen A, Wahlund KG. Zone broadening and dilution in rectangular and trapezoidal asymmetrical flow field-flow fractionation channels. Anal. Chem. 1991. 63: 1001–1007.
6. Qureshi RN, Kok WTh. LG/GC Eur. 2010. 23: 18-24.
7. Dinnebier RE, Billinge SJL. Powder Diffraction – Theory and Practice. Edited by R. E. Dinnebier and S. J. L. Billinge. RSC Publishing, Cambridge, 2008.
8. Rietveld HM. A profile refinement method for nuclear and magnetic structures. J. Appl. Cryst. 1969. 2: 65-71.
9. Coelho AA. 2012. TOPAS-Academic V5. Available at: http://www.topas-academic.net/
10. Balzar D, Audebrand N, Daymond MR, Fitch A, Hewat A, Langford JI, Le Bail A, Louër D, Masson O, McCowan CN, Popa NC, Stephens PW, Toby BH. Size-strain line-broadening analysis of the ceria round-robin sample. J. Appl. Cryst. 2004. 37: 911-924.

11. Beale AM, Weckhuysen BM. EXAFS as a tool to interrogate the size and shape of mono and bimetallic catalyst nanoparticles. Phys. Chem. Chem. Phys. 2010. 12: 5562-5574.
12. Dent AJ, Cibin G, Ramos S, Parry SA, Gianolio D, Smith AD, Scott SM, Varandas L, Patel S, Pearson MR, Hudson L, Krumpa NA, Marsch AS, Robbins PE. Performance of B18, the Core EXAFS Bending Magnet beamline at Diamond. Journal of Physics Conference Series 2013. 430: 1-7.
13. Ravel B, Newville M. ATHENA ARTEMIS HEPHAESTUS: Data analysis for X-Ray Absorption Spectroscopy using IFEFFIT. J. Synchroton. Rad. 2005. 12: 537-571.